Article

Air Mass Flow and Pressure Optimisation of a Pem Fuel Cell Hybrid System for a Forklift Application

Gojmir Radica , Ivan Tolj * , Mykhaylo Lototskyy , Sivakumar Pasupathi

Posted Date: 7 November 2023

doi: 10.20944/preprints202311.0407.v1

Keywords: Air mass flow; pressure; optimization; PEM fuel cell

Article

Air Mass Flow and Pressure Optimisation of a PEM Fuel Cell Hybrid System for a Forklift Application

Gojmir Radica [1], Ivan Tolj [2,*], Mykhaylo Lototsky [3] and Sivakumar Pasupathi [3]

[1] University of Split, Faculty of Electrical Engineering, Mechanical Engineering and Naval Architecture, Department of Thermal Machines, R. Boškovića 32, 21000 Split, Croatia
[2] University of Split, Faculty of Electrical Engineering, Mechanical Engineering and Naval Architecture, Department of Thermodynamics, R. Boškovića 32, 21000 Split, Croatia
[3] HySA Systems Competence Centre, South African Institute for Advanced Materials Chemistry (SAIAMC), University of the Western Cape, Bellville, South Africa
* Correspondence: itolj@fesb.hr

Abstract: A study was conducted on the power system of a forklift equipped with PEM fuel cells. A fuel cell assembly relies on several components for proper functioning, and among these, the air compressor holds paramount importance due to its significant energy consumption when compared to other Balance of Plant components. The air supply system, in turn, plays a critical role in ensuring the stable and efficient operation of the entire fuel cell system. To enhance system efficiency, we delved into the impact of varying the stoichiometric ratio of air and air pressure on the validated and optimized power module model. This investigation was carried out under real loading conditions, replicating the conditions experienced by the power module when fuel cells are in use within a forklift. The air compressor, being a pivotal component of a PEM fuel cell system, can be operated at different excess air and pressure ratios, which in turn influence both the fuel cell's performance and the overall efficiency of the power module system. Our research focused on assessing the performance of polymer electrolyte membrane (PEM) fuel cells under different load cycles, adhering to the VDI60 requirements for forklift applications. This comprehensive examination encompassed the system's minimum and maximum load scenarios, with the primary goal of optimizing excess air and pressure ratio parameters, especially under dynamic load conditions. The results revealed that higher air pressures and lower excess air ratios were conducive to increasing system efficiency, shedding light on potential avenues for enhancing the performance of PEM fuel cell systems in forklift applications.

Keywords: air mass flow; pressure; optimization; PEM fuel cell

1. Introduction

Clean hydrogen has the potential to meet up to 24% of the world's energy demand. As the global community, including the European Union, commits to reducing reliance on fossil fuels, hydrogen is emerging as a versatile solution for converting renewable energy from sources like wind and solar into storable forms. Hydrogen can serve as a feedstock, fuel, energy carrier, and storage medium, offering numerous applications across industries, transportation, power generation, and construction [1]. In the realm of zero-emission vehicle technologies, there are two prominent developments: battery-powered electric vehicles using lithium-ion batteries exclusively, and fuel cell vehicles employing compressed hydrogen tanks and proton exchange membrane (PEM) fuel cells to generate electricity from hydrogen gas [2]. In the context of fuel cell assemblies, one crucial and energy-intensive component is the air compressor [3]. Generally, higher airflow enhances fuel cell voltage and efficiency [4], while lower mass flows can lead to operational challenges like water condensation and insufficient oxygen supply [5]. High-velocity airflow is essential for removing water produced on the cathode side of the fuel cell, and it also increases oxygen partial pressure, thereby boosting fuel cell voltage [6]. However, extended operation at high airflow rates can lead to insufficient membrane moisture and potential drying issues [7]. The concept of the excess air ratio is vital, representing the ratio of actual airflow through the air compressor to the stoichiometric airflow required for complete oxygen consumption within the system [8]. Typical values range from 1.5 to 3.0, depending on system parameters and design considerations [9]. Furthermore, the pressure within the fuel cell system is influenced by the ratio of air compressor pressure to the pressure drop across the fuel cell [10]. When using a throttle valve after the fuel cell assembly, it may lead to increased pressure resistance and cathode side pressure [11]. Alternatively, employing an expander (turbine) in place of a throttle valve allows for the

 doi:10.20944/preprints202311.0407.v1

utilization of the energy from the pressurized air mass flow, enhancing system efficiency [12]. The air supply system is of utmost importance for ensuring the stable and efficient operation of the fuel cell system [13]. Proper air supply system operation aids in moisture removal, impacting humidity levels, while the oxygen content in the air directly affects fuel cell voltage and efficiency. The air compressor can supply air at various flow rates and pressure levels to the chimney, and these operational parameters, along with the corresponding electricity consumption of the compressor, significantly influence system efficiency [14]. The maximum inlet air pressure in the fuel cell is constrained by the surging line of the air compressor [15], while the lowest pressure is determined by the pressure drop of the fuel cell and the air compressor's choke. It's essential to avoid operating points below the choke line and above the surging line to prevent compressor damage due to overheating, high pressure, and pressure fluctuations [16]. Higher reactant pressures result in increased fuel cell voltage, power, and efficiency [18]. Typically, for PEM fuel cells, the voltage increase diminishes when the operating pressure exceeds 4 bar due to mass transfer limitations. Therefore, the optimal operating pressure for PEM fuel cells typically falls between 3 and 4 bar [19]. Research has suggested that an operating pressure of 2 bar yields optimal system efficiency, especially when using a screw compressor [20]. A study has investigated the impact of different pressure levels and excess air ratios on net cell voltage levels, utilizing the Nernst equation [21]. The optimal point was identified at 2 bar for an excess air ratio of 2. For excess air ratios exceeding 3, the net stress level was found to be negative. In another study [22], an 80 kW fuel cell vehicle was analyzed concerning blower speed and back pressure control valve. It was observed that at low loads, system power decreases as the regulating pressure valve angle increases (opens), with the influence of blower speed being more significant at higher valve angles. At high loads, for most fan speeds, system power increases when the back pressure valve opens and reaches a maximum before decreasing again if the valve is opened further. This behavior can be attributed to the modeled humidity inside the stack, affected by both blower speed (excess air ratio) and back pressure level. Furthermore, research into air mass flow and pressure optimization for PEM systems for fuel cell range extension found that various factors, such as feed gas humidity, operating temperature, feed gas stoichiometry, air pressure, fuel cell size, and gas flow patterns, affect both steady-state and dynamic fuel cell responses. The air stoichiometric flow rate directly influences fuel cell performance by supplying oxygen and indirectly by affecting membrane humidity and water flooding in the cathode side [24]. For air pressures exceeding 1.8 bar(a), the fuel cell stack's power gain due to pressurization is offset by the increased power required for air compression [25]. The optimization of super-high-speed electric air compressors for hydrogen fuel cell vehicles is a subject of investigation [26]. This paper assesses the optimal system efficiency of a PEM fuel cell system at different load points. The novelty of this work lies in the verified model development and combined investigation of air pressure and air mass flow on the system efficiency of an 11 kW power module with a PEM fuel cell designed for forklift applications. The study analyzes the trade-off between higher oxygen partial pressure inside the stack (resulting in higher efficiency) and the additional power consumption of the air compressor (leading to lower efficiency) for two distinct load points. To achieve this, a power module with a fuel cell stack model was developed and validated using experimental data obtained during forklift operations under VDI60 load cycles in real-world conditions. Simulations encompass various parameters of air mass flow and air pressure to assess their impact on system efficiency. Additionally, all models employed in the study were verified against measured data to ensure reliable simulation results.

2. Materials and Methods

In this study, a combination of experimental and theoretical methods was employed for the investigation. Firstly, the setup and components of the fuel cell system test bench are detailed. Secondly, the modeling methodology and the equations used for the theoretical investigations are explained. The forklift under examination is equipped with a fuel cell power module that incorporates CGH2 hydrogen storage at a pressure of 350 bar. This power module can deliver an output voltage of 80 VDC, with a maximum continuous current of 125 A. Furthermore, the power module was integrated with a metal hydride hydrogen storage extension tank, resulting in a hybrid CGH2 MH hydrogen storage system for the forklift [27].

Figure 1. shows simplified schematics of the equipment installed on-board the forklift in the configuration “fuel cell MH tank”, including fuel cell power module and the MH extension tank.

Preprints (www.preprints.org) | NOT PEER-REVIEWED | Posted: 7 November 2023 doi:10.20944/preprints202311.0407.v1

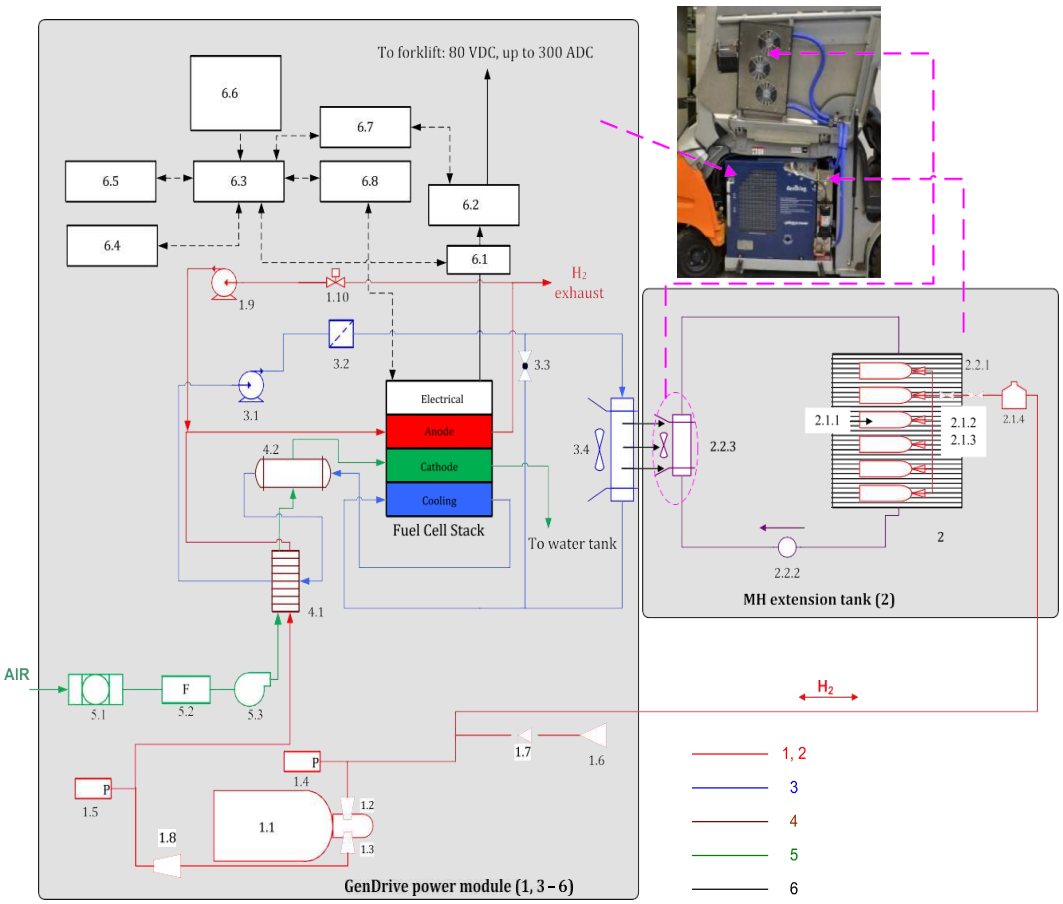

Figure 1. Simplified schematics of the on-board system. 1 hydrogen storage and supply subsystem: 1.1 gas cylinder, 1.2, 1.3 e adapters, 1.4, 1.5 pressure sensors, 1.6 refuelling receptacle, 1.7 check valve, 1.8 reducer, 1.9 recirculation pump, 1.10 purge valve. 2 MH extension tank: 2.1 hydrogen subsystem: 2.1.1 MH containers, 2.1.2, 2.1.3 shut-off valves, 2.1.4 gas filter; 2.2 thermal management subsystem: 2.2.1 water tank, 2.2.2 circulation pump, 2.2.3 radiator. 3 FC stack cooling subsystem: 3.1 coolant pump, 3.2 DI filter, 3.3 bypass valve, 3.4 radiator. 4 fuel/oxidant conditioning: 4.1 reactants conditioner, 4.2 humidifier assembly. 5 air supply subsystem: 5.1 filter, 5.2 flow meter, 5.3 compressor. 6 electrical components: 6.1 contactor, 6.2 Li-ion battery, 6.3 system master controller, 6.4 compressor motor controller, 6.5 cell voltage monitor, 6.6 BoP sensors (H2, tilt, coolant temperature, oxidant and fuel temperatures), 6.7 battery sensors (voltage, current, SoC), 6.8 stack sensors (voltage, current, temperature).[27].

Power consumption by balance of plant components of the fuel cell power module is presented in Table 1 [27].

Table 1. Power consumption by BoP components of the FC power module with MH extension tank.

Component	Contribution in the power consumption [W]
Power module electronics	143.6
Other BoP components of the power module providing FC stack operation	1058.8
MH thermal management system	313.8
TOTAL	1516.2

2.1. Stoichiometric Ratio

The excess air ratio represents the mass flow of air that actually flows through the stack, divided by the mass flow of air that would be required if all the oxygen were consumed by reaction inside the chimney (stoichiometric mass flow of air). Typical values of the excess air ratio are between 1.5 and 3.0, depending on system parameters and design.

The mass flow of the reacted hydrogen and oxygen can be calculated by [28].

Preprints (www.preprints.org) | NOT PEER-REVIEWED | Posted: 7 November 2023 doi:10.20944/preprints202311.0407.v1

$$m_{reacted,H_2} = \frac{I_{stack} * n_{cells}}{4 * F} * M(H_2) \quad (1)$$

And

$$m_{reacted,O_2} = \frac{I_{stack} * n_{cells}}{4 * F} M(O_2) \quad (2)$$

where M(H_2) and M(O_2) are the molar mass of hydrogen and oxygen. Using the stoichiometric ratio, the mass flow of total amount of hydrogen and oxygen fed to the fuel cell is equal to

$$m_{flow,H_2} = m_{reacted,H_2} * SR_{H_2} \quad (3)$$

and

$$m_{flow,O_2} = m_{reacted,O_2} * SR_{O_2} \quad (4)$$

The mass flow of the demanded air fed to the cathode of the fuel cell is equal to:

$$m_{flow,air} = \frac{I_{stack} * n_{cells} * M(Air)}{4 * F * O_2(Air)} \quad (5)$$

where M(Air) and O_2(Air) are the average molar mass of the air and the oxygen constitute in the air, respectively.

2.2. Compressor Pressure

The pressure inside the fuel cell is determined by the ratio of the air compressor pressure to the pressure drop through the fuel cell.

In the compressor model embedded in the fuel cell system, the outlet gas pressure is calculated as [28,29]

$$p_{out} = p_{in} * \Pi \quad (6)$$

where the two terms on the right hand side of the equation are the inlet gas pressure of the compressor and the pressure ratio, respectively. The outlet gas temperature is

$$T_{out} = T_{in} * \Pi^{\frac{k_{gas}-1.0}{k_{gas}}} \quad (7)$$

where Tin and kgas are the inlet gas temperature and the ratio of the heat capacity at a constant pressure to the heat capacity at a constant volume[25]. The power consumption of the compressor is expressed as:

$$P_{compressor} = m_{flow,in} * \frac{1}{n_{s,C}} * c_p * T_{in} * \left[\Pi^{\frac{k-1}{k}} - 1\right] \quad (8)$$

where mflow,in, ns,C and cp are the mass flow of the compressor inlet, isentropic efficiency of the compressor and mean value of the specific heat at constant pressure between the compressor inlet and outlet, respectively. When the compressor operates at its idle speed, its inlet mass flow is equal to its idle mass flow. Otherwise, when higher gas pressure is required from the fuel cell stack, its inlet mass flow is:

$$m_{flow,in} = m_{flow,air} \quad (9)$$

2.3. Power

The power of the fuel cell is defined as [28,29]

$$P_{cell} = U_{cell} * I_{stack} \quad (10)$$

and the power loss of the fuel cell is

$$P_{loss,cell} = (U_{oc} - U_{cell}) * I \quad (11)$$

The corresponding efficiency of the fuel cell is

Preprints (www.preprints.org) | NOT PEER-REVIEWED | Posted: 7 November 2023 doi:10.20944/preprints202311.0407.v1

$$\eta_{cell} = \left(\frac{U_{oc} - U_{cell}}{U_{oc}}\right) \tag{12}$$

The power of the compressor can be fed into the electric system with the compressor current:

$$I_{compresor} = \frac{P_{compresor}}{U_{compresor}} \tag{13}$$

3. Fuel Cell Hybrid Power pack Model

Figure 2 illustrates a schematic of the power pack utilized in lift trucks, combining both a fuel cell system (FCS) and a battery. The battery is directly linked to the DC bus, while the FCS is connected to the bus via a unidirectional DC/DC converter, facilitating precise control over the FCS's power output. Additionally, a bidirectional DC/DC converter precedes the battery, functioning at different voltage levels and providing the capability to manage power effectively. This bidirectional operation allows for both discharging and charging of the battery.

This topology, as depicted in Figure 2, represents the conventional approach employed in lift trucks, as documented in the literature (reference [27]). It is favored for its numerous advantages over alternative topologies. Notably, in this configuration, the DC bus voltage aligns with the battery voltage, eliminating the need for direct bus voltage regulation.

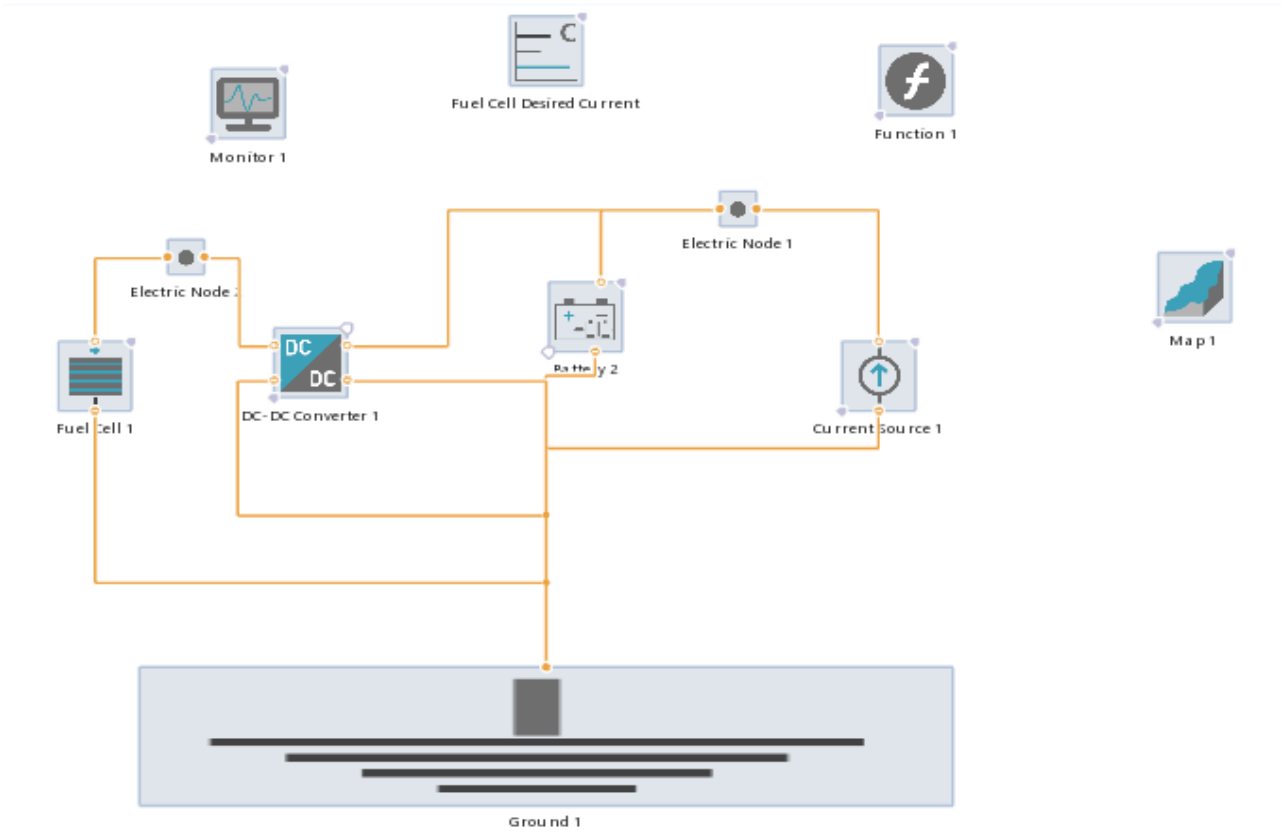

Figure 2. PEM Fuel Cell- Battery Power Pack Model.

The fuel cell model is constructed upon analytical electrochemical equations derived from the polarization curve observed on the cathode side of the Proton Exchange Membrane Fuel Cell (PEMFC). This model offers an approximate solution that factors in oxygen and proton transport losses occurring in the Catalyst Coated Layer (CCL), as well as oxygen transport losses within the Gas Diffusion Layer (GDL). It accounts for variations in temperature, relative humidity, and gas pressure on the cathode side.

Preprints (www.preprints.org) | NOT PEER-REVIEWED | Posted: 7 November 2023 doi:10.20944/preprints202311.0407.v1

This versatile model serves the purpose of assessing both electrical characteristics, such as voltage, power output, power losses, and efficiency of the fuel cell, as well as gas-related properties, such as the total consumption of oxygen and hydrogen. Moreover, within the fuel cell component, there exists the option to activate a simplified compressor model. This inclusion allows for the consideration of the compressor's power consumption, a critical factor significantly impacting the operational efficiency of the entire fuel cell system. Key properties of the fuel cell are detailed in Table 2.

Table 2. Fuel cell properties.

Layout Configuration		
Number of cells in a stack:	75	
Fuel Cell Properties		
Cell area:	370	cm^2
CCL proton conductivity:	3	A / (V·m)
Ideal open circuit voltage:	1.23	V
Tafel slope:	0.03	V
Catalyst layer thickness:	0.001	cm
GDL thickness:	0.02	cm
Maximum current:	1000	A
Cathode Gas Properties		
Oxygen constitute:	21	%
Initial Conditions		
Cathode inlet gas pressure:	2	bar
Relative humidity:	70	%

The term "Oxygen constitute" refers to the purity level of oxygen in the gas supplied to the cathode at its inlet. Meanwhile, "Cathode inlet gas pressure (absolute)" represents the absolute gas pressure measured at the entrance of the cathode. It's important to note that if an internal compressor is employed in the system, this input parameter would be substituted by the outlet pressure of the compressor.

The operational parameters encompass temperature, pressure, relative humidity, and the stoichiometric ratio of the reactant gases. These variables play a pivotal role in shaping the system's performance.

Moreover, the system's load profile adheres rigorously to the established standards detailed in VDI 60 for material handling applications, as visually presented in Figure 4. This profile offers a well-structured representation of the system's operation across diverse conditions and serves as a fundamental tool for assessing its real-world performance.

Preprints (www.preprints.org) | NOT PEER-REVIEWED | Posted: 7 November 2023 doi:10.20944/preprints202311.0407.v1

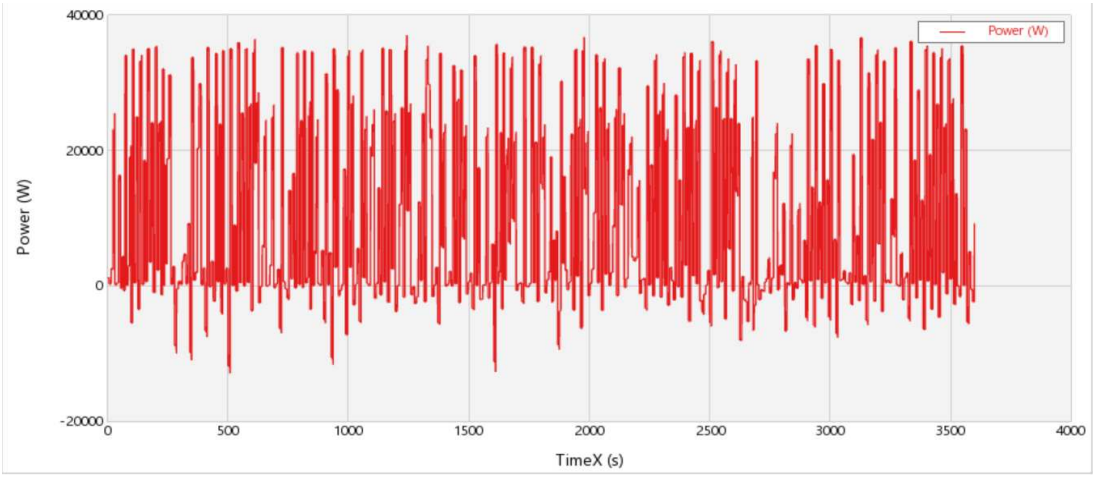

Figure 3. VDI 60 Load profile.

Heavy-duty tests of the forklift were carried out according to VDI 60/VDI 2198 standard protocol. Note the duration of driving/lifting/dropping cycle was ~1 min (60 cycles per 1 h) and the distance, L, between lifting/dropping points was of 30 m.

4. Results and Discussion

In this chapter, we will present the simulation results. To effectively incorporate the hybrid functionalities into the forklift, we employed the AVL - Cruise M program. Before initiating the simulation, it's crucial to establish the driving conditions to which the vehicle will be subjected. Based on these conditions, we select the appropriate driving cycle. Driving cycles provide a description of the real-world loads that the vehicle may encounter during operation. Figure 5 highlights the key characteristics associated with default values for this purpose.

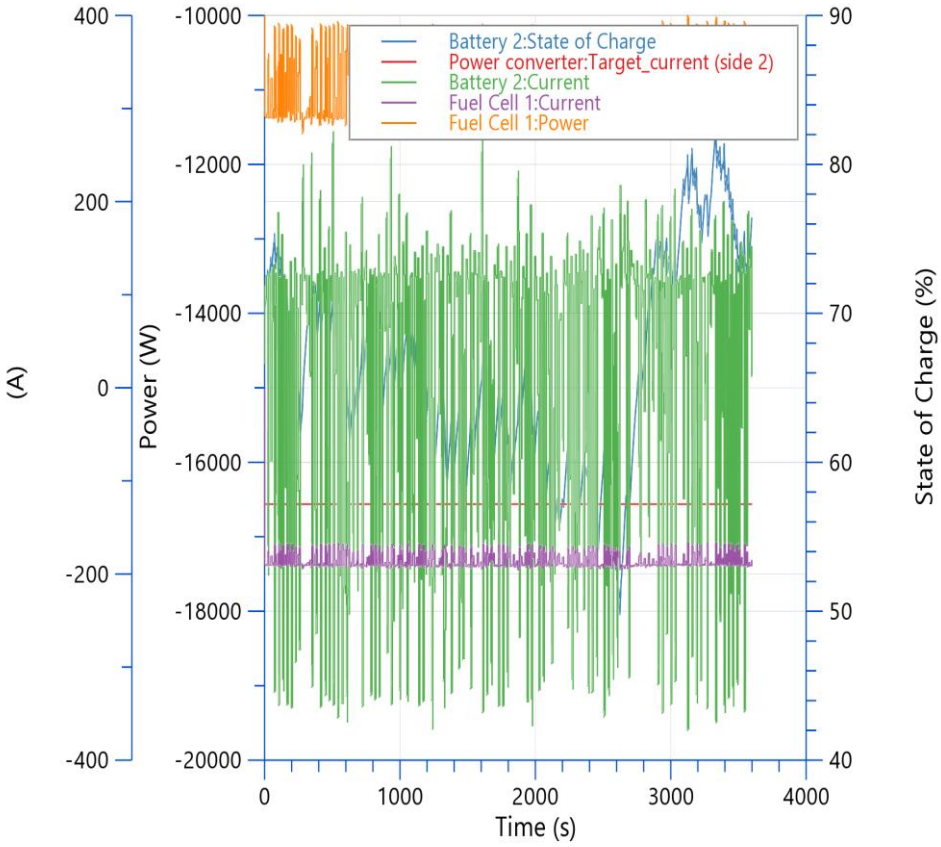

Figure 4. Simulation 1 - Battery capacity 25Ah, fuel cell power 11kW FC:75cells_370mm2;Bat.:75V 25Ah; Current -125A.

Preprints (www.preprints.org) | NOT PEER-REVIEWED | Posted: 7 November 2023 doi:10.20944/preprints202311.0407.v1

The stack comprises 75 fuel cells, each with a cell area of 370 square millimeters. The battery operates at a voltage of 75 volts and possesses a rated capacity of 25 ampere-hours (Ah). Under default conditions, the current is set at 125 amperes (A), which maintains the fuel cell's power output at 11 kilowatts (kW). Notably, the state of charge (SOC) of the battery remains at a reasonable level throughout the operation.

When the battery's SOC reaches 50%, the fuel cell begins supplying power to the battery. Conversely, when the SOC reaches 82%, the fuel cell ceases its operation. Importantly, the fuel cell maintains a stable output current throughout the operation, and its power output gradually adjusts to match the load power request, effectively mitigating the impact of abrupt load changes on the fuel cell. The battery's charging and discharging follow the load's power requirements.

The reacted hydrogen mass flow ranges between 0.13 grams per second and 0.15 grams per second. When recalculated under "normal" conditions, this translates to an amount between 10 normal liters per minute (Nl/min) and 15 Nl/min per 1 kilowatt, as illustrated in Figure 6. In total, the reacted hydrogen mass amounts to 0.45 kilograms.

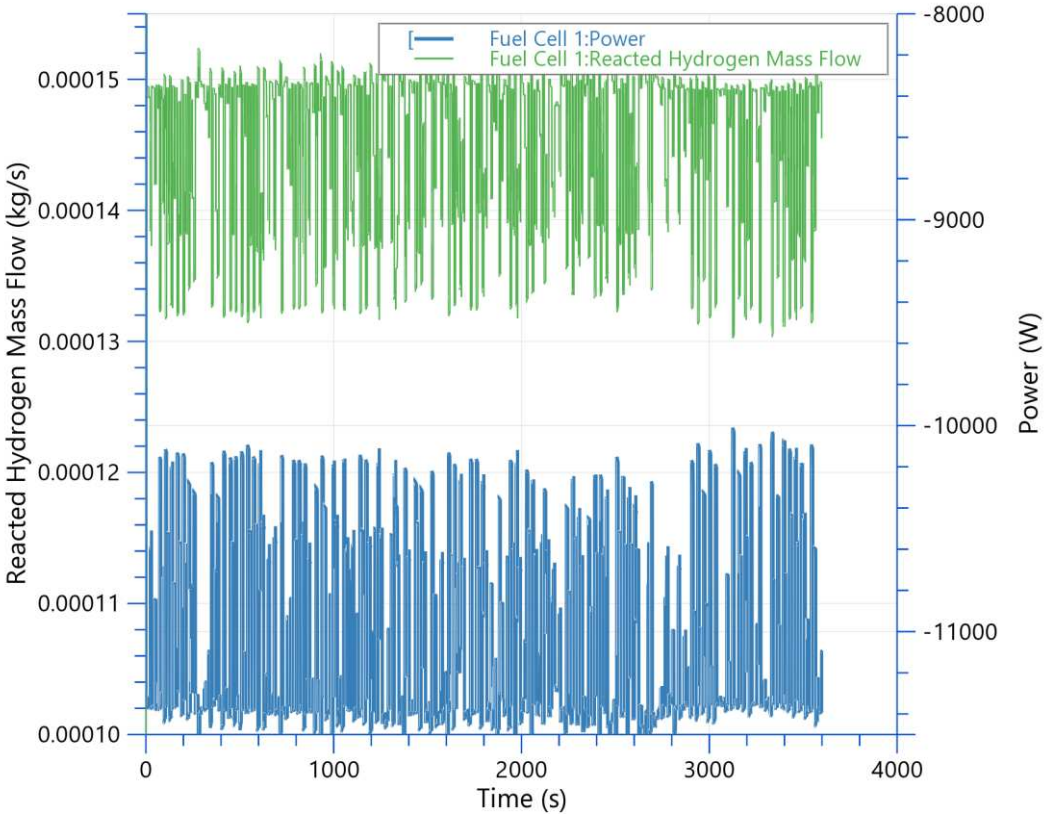

Figure 5. Reacted Hydrogen Mass Flow (kg/s).

4.1. Design of Experiment

The Design of Experiment (DOE) gives a selection of design points, for which the numerical simulations should be evaluated. It is necessary to find good starting points for the optimization process. DoE called space filling design is preferred for the search of a good starting design for the optimization.

Design of Experiment is performed with following Input/Output parameters:

Table 3. DOE input-output parameters.

Correlate parameters	Input/Output
Stoichiometric ratio oxygen	Input
Target pressure ratio	Input
Compressor Power Mean	Output
Cumulated Hydrogen Mass Consumption	Output

Preprints (www.preprints.org) | NOT PEER-REVIEWED | Posted: 7 November 2023 doi:10.20944/preprints202311.0407.v1

Energy Consumption	Output
Objective	Output

The input parameters comprise the Oxygen Stoichiometric ratio and the Air pressure ratio. The primary objectives are to minimize energy consumption and hydrogen usage. The obtained results indicate that these objectives are successfully attained at pressure ratios of 2.5 and Stoichiometric ratios of 2.8 and 3, as detailed in Table 4 and illustrated in Figure 6.

Table 4. DOE input-output parameters with objectives.

Target_pressure...	Stoichiometric_...	Feasibility	CompressorPo...	ReactedHydrog...	Objective	Training data	Status	Progress
2.5	3	0	1491.058733	0.514673	30.940791	☑	completed	100 %
2.5	2.8	0	1393.085906	0.515203	17.433425	☑	completed	100 %
2.5	2.5	0	1246.199349	0.516185	6.132163	☑	completed	100 %
2	3	0	1097.211435	0.517499	2.348649	☑	completed	100 %
2.5	2	0	1001.712337	0.518646	1.880059	☑	completed	100 %
2	2.5	0	917.364924	0.519209	1.495363	☑	completed	100 %
2	2	0	737.859371	0.522016	0.96	☑	completed	100 %
1.5	3	0	621.435187	0.522639	0.835815	☑	completed	100 %
1.5	2.5	0	519.94697	0.524743	0.732348	☑	completed	100 %
1.5	2	0	418.734339	0.528246	0.637172	☑	completed	100 %

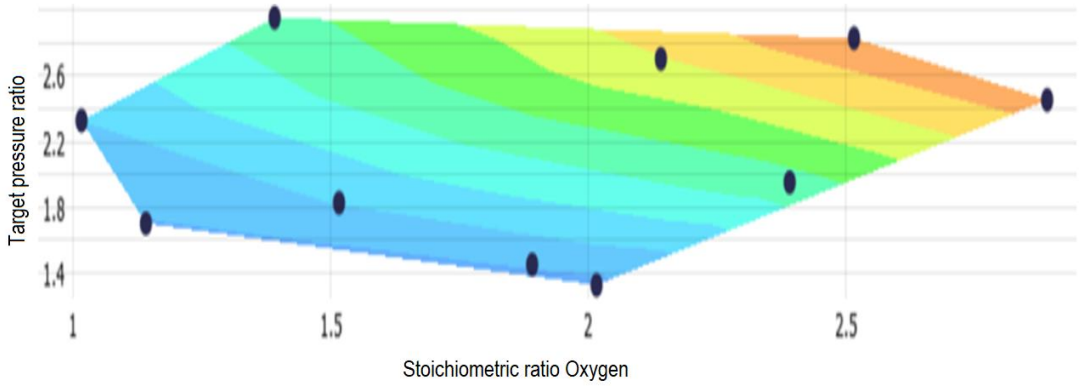

Figure 6. DOE results with air pressure ratio and Stoichiometric ratio of Oxygen.

The compressor power at optimized load is 1491 W and Hydrogen consumption is 0.51 kg during simulated VDI60 load cycle.

4.2. The Nelder-Mead Optimization Algorithm

The Nelder-Mead optimization algorithm, or simplex search algorithm, is used for multidimensional unconstrained optimization. The method does not require any derivative information, which makes it suitable for problems with non-smooth functions.

Following objectives are defined: Energy Consumption, Cumulated Hydrogen Mass Consumption and Mean Compressor Power.

For the Nelder-Mead optimization algorithm, following variables are determined and analyze: Oxygen Stoichiometric Rate (in range 2-3) and Pressure Rate (in range 1.5-3) suggested by results obtained with DOE analyze.

Design points for optimization are defined by the Sobol sequence (Table 5.), which is a quasi-random sequence, due to their common use as a replacement of uniformly distributed random numbers. The advantage of this method is that a great part of the design space is covered by a small number of design points.

Preprints (www.preprints.org) | NOT PEER-REVIEWED | Posted: 7 November 2023 doi:10.20944/preprints202311.0407.v1

Table 5. Design points for optimization (defined by the Sobol sequence).

	Feasibility	Stoichiometric_ratio_oxygen ([-])	Target_pressure_ratio ([-])
1	0	2.914062	2.636719
2	0	2.414062	1.886719
3	0	2.164062	2.261719
4	0	2.664062	1.511719
5	0	2.726562	2.917969
6	0	2.226562	2.167969
7	0	2.476562	2.542969
8	0	2.976562	1.792969
9	0	2.851562	2.355469
10	0	2.351562	1.605469

Optimization gives following optimum results (Figure 7.):

- Energy Consumption 60,426 kJ or (16,785kWh)
- Cumulated Hydrogen Mass Consumption 0.5143 kg
- Mean Compressor Power 1,543.68 W

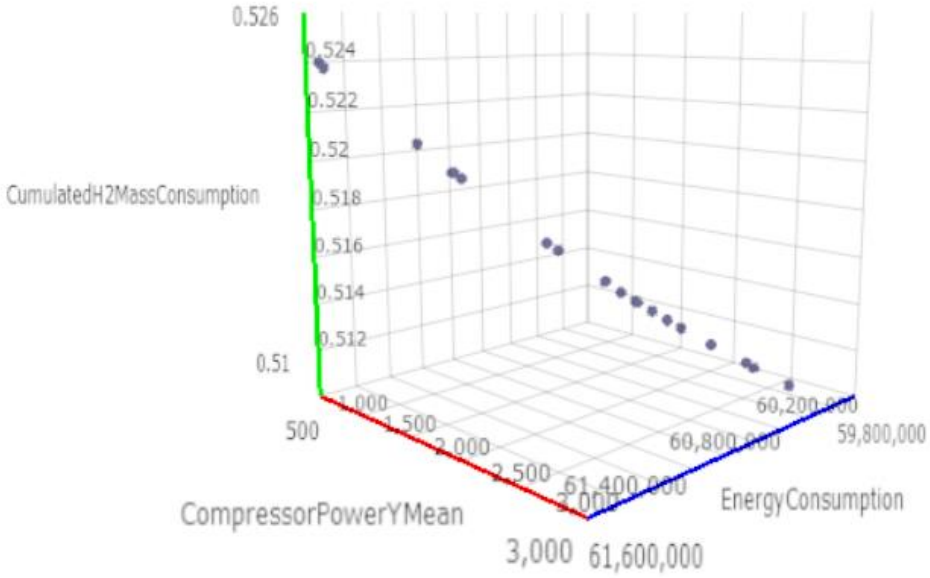

Figure 7. Optimisation results with dependency on three inputs: Energy Consumption (J), Cumulated Hydrogen Mass Consumption (kg) and Mean Compressor Power (W).

The highest objective is achieved with pressure ratio: 1.512 and Oxygen Stoichiometric ratio: 2.7266 (Figure 8).

Preprints (www.preprints.org) | NOT PEER-REVIEWED | Posted: 7 November 2023 doi:10.20944/preprints202311.0407.v1

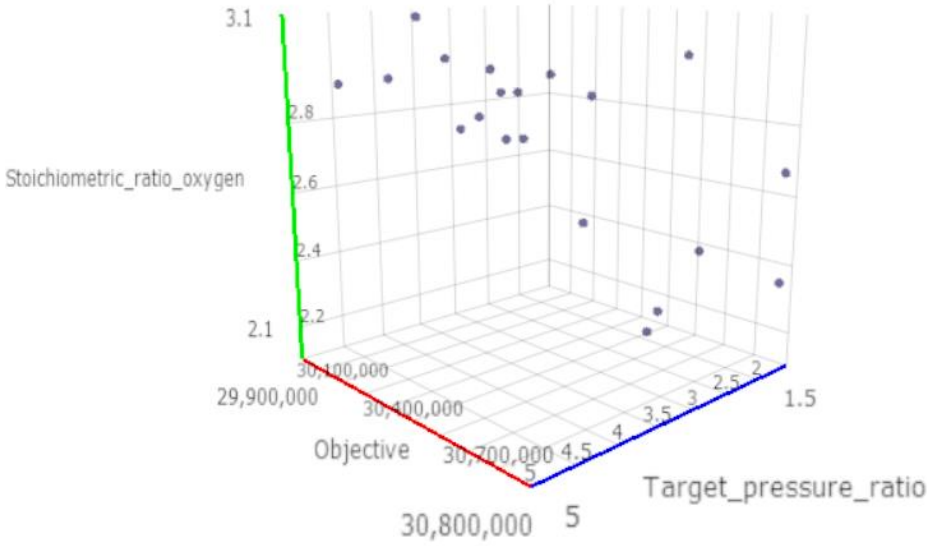

Figure 8. Optimization results with air pressure ratio and Stoichiometric ratio of Oxygen.

4.3. Analyse of the Air Excess Ratio and the Pressure Ratio Influencing Parameters

Here is the analyze of the system's minimum and maximum load scenarios, with the primary goal of optimizing excess air and pressure ratio parameters, especially under dynamic load conditions. The air compressor has the capability to deliver varying air mass flows and air pressure levels to the stack, and these operational parameters directly impact the electric energy consumption of the compressor, subsequently influencing the overall efficiency of both the stack and the system. This study is focused on optimizing system efficiency with respect to air supply parameters, specifically the air excess ratio and pressure ratio.

Numerous simulations were conducted, exploring different combinations of air pressures and air excess ratios to enhance the system's performance. The primary objective is to optimize fuel cell performance while understanding the individual impacts of each parameter on fuel cell efficiency, hydrogen consumption, and power loss. In this report, we present key findings from these simulations.

The first simulation was conducted with an air excess ratio of 2 and a pressure ratio 1.9 (which is actually 1,9 bar as initial pressure is 1 bar), with results detailed in Table 6, Figure 9, and Figure 10. The analysis provides insights for two distinct points in time, denoted as Time 1 and Time 2, representing conditions that maximize and minimize compressor power or system power loss.

Table 6 displays several crucial parameters, including H2Mass (the mass of hydrogen consumed during the VDO 60 load cycle, lasting 3600 seconds), Pcomp (the power of the air compressor), Eta (the fuel stack efficiency), and Power loss (the sum of all losses in the system). Additionally, we have included the following derived parameters: Air mass, Air mass flow, oxygen mass flow, and hydrogen mass flow, all presented at two distinct moments, and differences are calculated for each parameter.

The results show that the fuel cell efficiency varied between 65% and 64%, the compressor power ranged from 627 W to 701 W, and hydrogen mass varied from 0.391 kg to 0.396 kg.

Table 6. Results with air excess ratio 2 and pressure ratio 1,9.

		Time 1	Time 2	Differences	Differences
Time	s	2693.6	2729.1		%
H_2Mass	kg	0.391	0.39631	-176.982	0.986601
Pcomp	W	627.6	701	-73.4	0.895292
Eta		0.65172	0.64613	0.00559	1.008652
Power loss	W	5491.6	6232.9	-741.3	0.881067
Air mass	kg	26.68971	27.05091	-0.3612	0.986647

Preprints (www.preprints.org) | NOT PEER-REVIEWED | Posted: 7 November 2023 doi:10.20944/preprints202311.0407.v1

Air mass flow	kg/s	0.00916	102316	-102316	8.95E-08
Oxygen mass flow	kg/s	0.91595	0.001187	0.914763	771.4562
Hydrogen mass flow	kg/s	0.000134	0.000151	-1.6E-05	0.891694

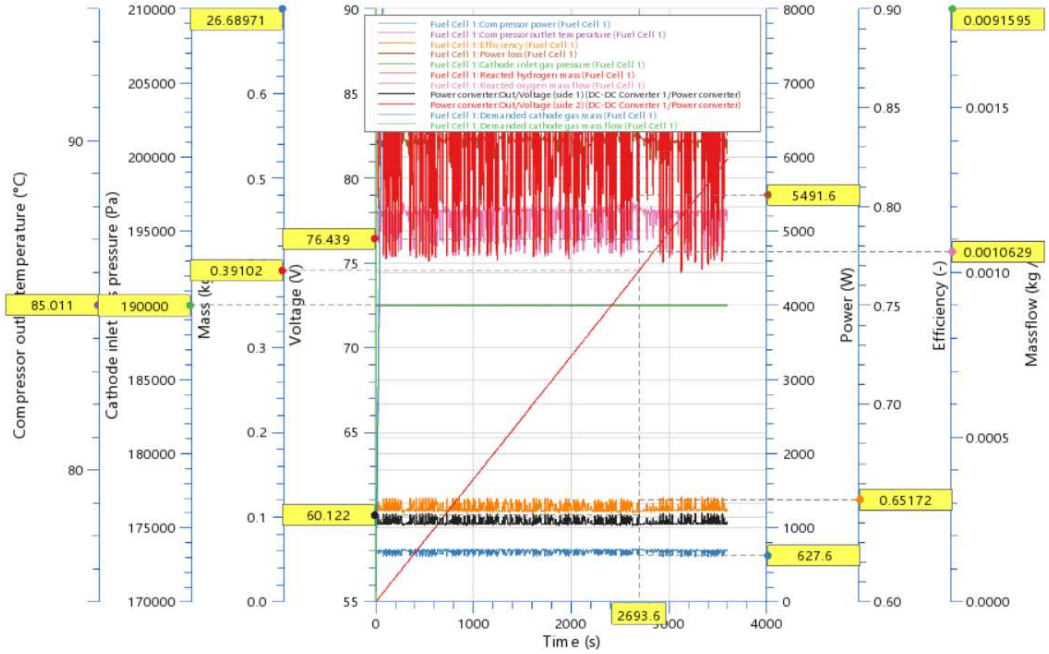

Figure 9. Obtain results with air excess ratio 2 and pressure ratio 1,9 at Time 1.

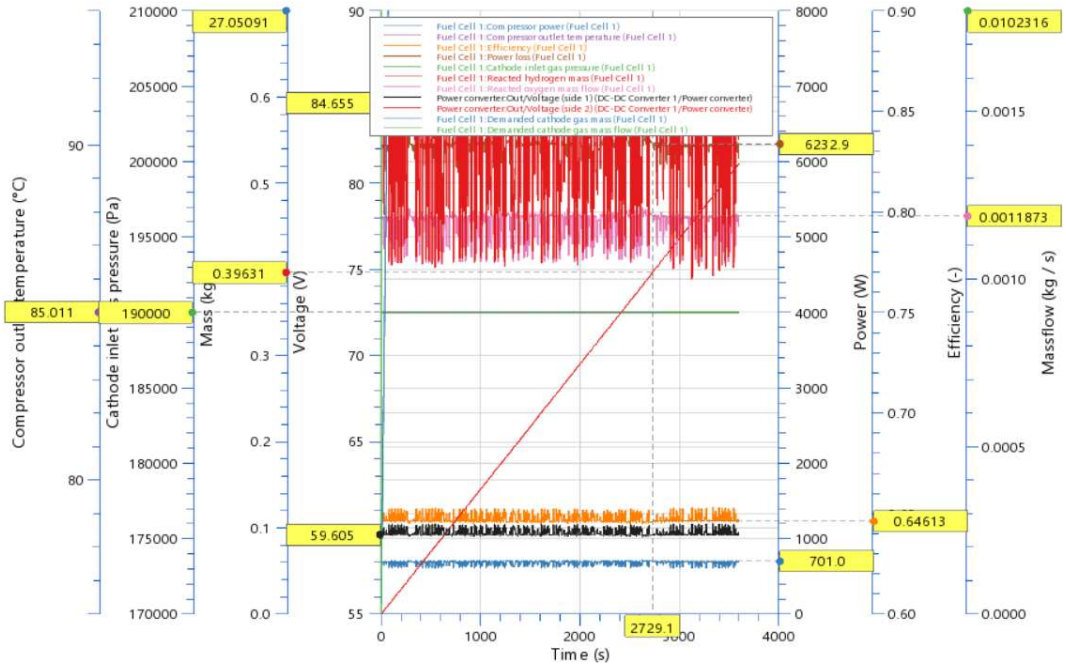

Figure 10. Obtain results with air excess ratio 2 and pressure ratio 1,9 at Time 2.

Second simulation is performed with air excess ratio 2 and air pressure 2 (bar) (table 7, Figure 11. and 12.). The efficiency varied from 65.3-64.7%, the compressor power varied from 681-761kW, and hydrogen mass varied from 0.39-0.3956kg

Preprints (www.preprints.org) | NOT PEER-REVIEWED | Posted: 7 November 2023 doi:10.20944/preprints202311.0407.v1

Table 7. Results with air excess ratio 2 and pressure ratio 2.

		Time 1	Time 2	Differences	Differences
Time	s	2693.6	2729.1	%	
H_2Mass	kg	0.39032	0.39561	-176.316	0.986628
Pcomp	W	681.8	761.4	-79.6	0.895456
Eta		0.65276	0.64733	0.00543	1.008388
Power loss	W	5466.6	6200.3	-733.7	0.881667
Air mass	kg	26.6423	27.00284	-0.36054	0.986648
Air mass flow	kg/s	0.009145	0.010213	-0.00107	0.895454
oxygen mass flow	kg/s	0.001061	0.001185	-0.00012	0.895452
hydrogen mass flow	kg/s	0.000134	0.00015	-1.6E-05	0.895722

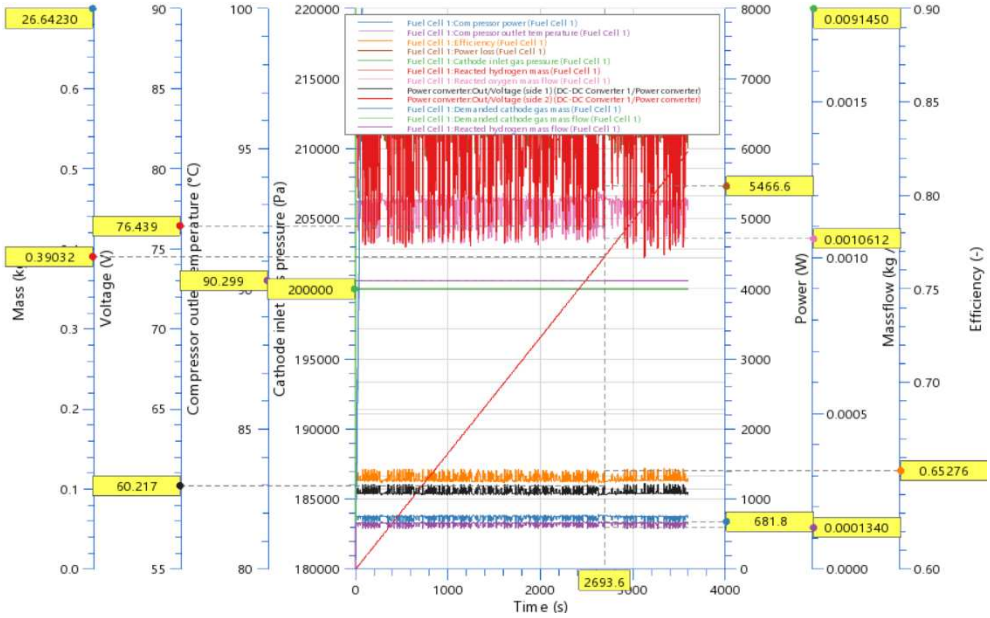

Figure 11. Obtain results with air excess ratio 2 and pressure ratio 2 at Time 1.

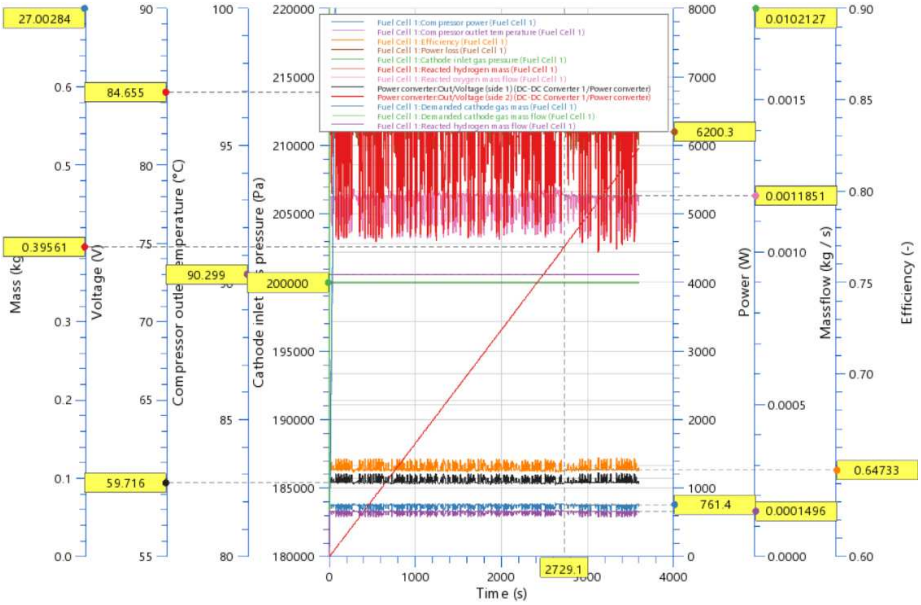

Preprints (www.preprints.org) | NOT PEER-REVIEWED | Posted: 7 November 2023 doi:10.20944/preprints202311.0407.v1

Figure 12. Obtain results with air excess ratio 2 and pressure ratio 2 at Time 2.

Third simulation is performed with air excess ratio 2 and air pressure 2.5 (bar) (table 8). The efficiency varied from 65.7-65.2%, the compressor power varied from 926-1033kW, and hydrogen mass varied from 0.388-0.39305kg. These parameters give the best fuel stack efficiency with the lowest hydrogen consumption.

Table 8. Results with air excess ratio 2 and pressure ratio 2.5.

		Time 1	Time 2)	Differences	Differences
Time	s	2693.6	2729.1		%
H2Mass	kg	0.38788	0.39305	-172.316	0.986846
Pcomp	W	926.3	1033.4	-107.1	0.896362
Eta		0.65655	0.6517	0.00485	1.007442
Power loss	W	5376.3	6082.2	-705.9	0.88394
Air mass	kg	26.68971	26.82859	-0.13888	0.994823
Air mass flow	kg/s	0.009093	0.010144	-0.00105	0.896413
oxygen mass flow	kg/s	0.001055	0.001177	-0.00012	0.896517
hydrogen mass flow	kg/s	0.000133	0.000149	-1.5E-05	0.896366

Fourth simulation is performed with air excess ratio 2.5 and air pressure 2 (bar) (table 9). The efficiency varied from 65.6-65.07%, the compressor power varied from 848-950kW, and hydrogen mass varied from 0.388-0.3925kg.

Table 9. Results with air excess ratio 2.5 and pressure ratio 2.

		Time 1	Time 2	Differences	Differences
Time	s	2694.1	2729.1		%
H2Mass	kg	0.38829	0.39254	-141.652	0.989173
Pcomp	W	848	950.1	-102.1	0.892538
Eta		0.6561	0.65071	0.00539	1.008283
Power loss	W	5387.1	6130.6	-743.5	0.878723
Air mass	kg	33.19267	33.49227	-0.2996	0.991055
Air mass flow	kg/s	0.011375	0.012745	-0.00137	0.892496
oxygen mass flow	kg/s	0.001056	0.001183	-0.00013	0.892486
hydrogen mass flow	kg/s	0.000133	0.000149	-1.6E-05	0.892236

Table 10. gives all results of simulation where it can be seen that with air stoichiometry 2 and air pressure ratio 2,5 the best value of parameters are obtain: highest fuel cell efficiency, lower hydrogen consumption and the lowest power loss. The only parameter that is better is at air stoichiometry 2.5 and air pressure ratio 2 at higher load point.

Preprints (www.preprints.org) | NOT PEER-REVIEWED | Posted: 7 November 2023 doi:10.20944/preprints202311.0407.v1

Table 10. Collective results of the simulation.

		s2p1,9	s2p1,9	s2p1,9	s2p1,9	s2p2	s2p2	s2p2	s2p2	s2p2,5	s2p2,5	s2p2,5	s2p2,5	s2,5p2	s2,5p2	s2,5p2	s2,5p2
Time	s	Time	Time 2	Differences	%	Time	Time 2	Differences	%	Time	Time 2	Differences	%	Time	Time 2	Differences	%
		2693.6	2729.1			2693.6	2729.1			2693.6	2729.1			2693.6	2729.1		
H_2Mass	kg	0.391	0.39631	0.00531	1.33986021	0.39032	0.39561	0.00529	1.3371755	0.38788	0.39305	0.00517	1.31535428	0.38829	0.39254	0.00425	1.08269221
Pcomp	W	627.6	701	73.4	10.4707561	681.8	761.4	79.6	10.4544261	926.3	1033.4	107.1	10.3638475	848	950.1	102.1	10.7462372
Eta		0.65172	0.64613	-0.00559	-0.865151	0.65276	0.64733	-0.0054	-0.8388303	0.65655	0.65017	-0.0049	-0.7442075	0.6561	0.65071	-0.0054	-0.828326
Power loss	W	5491.6	6232.9	741.3	11.8933402	5466.6	6200.3	733.7	11.8332984	5376.3	6082.2	705.9	11.6059978	5387.1	6130.6	743.5	12.1276873
Air mass	kg	26.6897	27.05091	0.3612	1.33526007	26.6423	27.0028	0.36054	1.33519289	26.6897	26.8286	0.13888	0.51765672	33.1927	33.4923	0.2996	0.89453477
Air mass flow	kg/s	0.00916	0.010232	0.0010716	10.4734352	0.00915	0.01021	0.00107	10.4572604	0.00909	0.01014	0.00105	10.3608044	0.01138	0.01275	0.00137	10.7493135
oxygen mass flow	kg/s	0.00106	0.001187	0.000127	10.6992418	0.00106	0.00119	0.00012	10.464135	0.00106	0.00118	0.00012	10.3653356	0.00106	0.00118	0.00013	10.7354184
hydrogen mass flow	kg/s	0.00013	0.000151	0.000017	11.2582781	0.00013	0.00015	1.6E-05	10.6666667	0.00013	0.00015	1.6E-05	10.738255	0.00013	0.00015	1.6E-05	10.738255
Fuel cell power	W	10100	11400	1300	11.4035088												

s-air stoichiometry; p- air pressure ratio.

 doi:10.20944/preprints202311.0407.v1

5. Conclusions

This paper presents the results of research into the influence of air stoichiometry and air pressure for power modules with PEM fuel cells. The simulations were performed on the optimized and validated model of the power module installed in the forklift. Airflow control is very important for a fuel cell system for transportation vehicles. Based on the model of a power module with fuel cells for a forklift, the influence of excess air and air pressure at different loads was analyzed. Several simulations are provided with different combinations of air pressures and air excess ratios to increase the system. The aim is to optimize the fuel cell performances and to see the influence of each parameter on fuel cell efficiency, hydrogen consumption and power loss. This research examined the system's minimum and maximum load scenarios, with the primary goal of optimizing excess air and pressure ratio parameters under dynamic load conditions.

The results show that with air excess ratio 2 and air pressure 2.5 (bar) the efficiency varied from 65.7-65.2%, the compressor power varied from 926-1033kW, and hydrogen mass varied from 0.388-0.39305kg. These parameters give the best fuel stack efficiency with the lowest hydrogen consumption. The only parameter that is better is at air stoichiometry 2.5 and air pressure 2 at higher load point.

Further research is needed to determine the impact of variable excess oxygen ratio and to conduct numerical and experimental investigation of a regulator capable of tracking the optimal performance of fuel cells when regulating excess oxygen ratio with different current disturbances/loads. As a future work, a controller of the optimal excess oxygen ratio will be established, in the power module with fuel cells in real load conditions.

Author Contributions: Conceptualization, G.R.; methodology, G.R.; software, G.R.; validation, G.R., I.T.; formal analysis, G.R., I.T.; investigation, G.R., I.T., M.V.L.; resources, G.R., I.T., M.V.L.; data curation, G.R., I.T., M.V.L.; original draft preparation, G.R.; writing, G.R., I.T., M.V.L.; visualization, G.R., I.T..; supervision, I.T., M.V.L project administration, I.T., M.V.L.; funding acquisition, G.R., I.T., M.V.L,.All authors have read and agreed to the published version of the manuscript.

Funding: This work has been fully supported by European Commission, Grant Agreement number: 778307 HYDRIDE4MOBILITY H2020 MSCA RISE 2017 "HYDRIDE4MOBILITY"support of international collaboration, and the Croatian Science Foundation under the project IP.2020-02-6249.

Data Availability Statement: The data used in this study are reported in the paper figures and tables.

Acknowledgments: The authors would like to thank HySA Systems, South African Institute for Advanced Materials Chemistry, University of the Western Cape for contribution in experimental research and AVL, Graz for software support.

Conflicts of Interest: The authors declare no conflict of interest.

References

1. https://www.eceee.org/all-news/news/eu-unveils-300-million-plan-to-fund-hydrogen-research/, EurActiv, 10 Mar 2022
2. Wu H-W. A review of recent development: transport and performance modeling of pem fuel cells. Appl Energy 2016;165:81e106.,https://doi.org/10.1016/j.apenergy.2015.12.075. http://www.sciencedirect.com/science/article/pii/S0306261915016487.
3. Cunningham JM, Hoffman MA, Moore RM, Friedman DJ. Requirements for a flexible and realistic air supply model for incorporation into a fuel cell vehicle (fcv) system simulation. SAE Trans 1999:3191e6.
4. Reshetenko TV, Bender G, Bethune K, Rocheleau R. Systematic study of back pressure and anode stoichiometry effects on spatial pemfc performance distribution. Electrochim Acta 2011;56(24):8700e10. https://doi.org/10.1016/j.electacta.2011.07.058. http://www.sciencedirect.com/science/article/pii/S0013468611011029 .
5. Matraji I, Laghrouche S, Jemei S, Wack M. Robust control of the pem fuel cell air-feed system via sub-optimal second order sliding mode. Appl Energy 2013;104:945e57. https://doi.org/10.1016/j.apenergy.2012.12.012.

6. Kulikovsky A. The effect of stoichiometric ratio on the performance of a polymer electrolyte fuel cell. Electrochim Acta 2004;49(4):617e25. https://doi.org/10.1016/j.electacta.2003.09.016.
7. Andjar J, Segura F. Fuel cells: history and updating. a walk along two centuries. Renew Sustain Energy Rev 2009;13(9):2309e22. https://doi.org/10.1016/j.rser.2009.03.015.http://www.sciencedirect.com/science/article/pii/S1364032109001336.
8. Ji SW, Myung NS, Kim TS. Analysis of operating characteristics of a polymer electrolyte membrane fuel cell coupled with an air supply system. J Mech Sci Technol,2011;25(4):945e55. https://doi.org/10.1007/s12206-011-0138-0.
9. Rabbani A, Rokni M. Dynamic characteristics of an automotive fuel cell system for transitory load changes. Sustain Energy Technol Assess 2013;1:34e43. https://doi.org/10.1016/j.seta.2012.12.003. http://www.sciencedirect.com/ science/article/pii/S2213138812000057.
10. Lang O, Pischinger S, Sch€onfelder C, Steidten T. Compressor expander units for mobile fuel cell systems. MTZ worldwide 2004;65(7):29e32. https://doi.org/10.1007/BF03227690
11. Boettner DD, Paganelli G, Guezennec YG, Rizzoni G, Moran MJ. Proton exchange membrane fuel cell system model for automotive vehicle simulation and control. J,Energy Resour Technol 2002;124(1):20e7. https://doi.org/10.1115/1.1447927.
12. Cunningham J, Hoffman M, Eggert A, Friedman D. The implications of using an expander (turbine) in an air system of a pem fuel cell engine. In: Proceedings of the 17th international electric vehicle symposium & exposition; 2000.
13. Pischinger S, Schonfelder C, Bornscheuer W, Kindl H, Wiartalla A. Integrated air supply and humidification concepts for fuel cell systems. SAE Trans 2001:86e92.
14. Jung G-B, Lo K-F, Su A, Weng F-B, Tu C-H, Yang T-F, Chan SH. Experimental evaluation of an ambient forced-feed airsupply opem fuel cell. Int J Hydrogen Energy 2008;vol.33(12):2980e5. https://doi.org/10.1016/j.ijhydene.2008.03.056.
15. T. Sun, X. Zhang, B. Chen, X. Liu, Coordination control strategy for the air management of heavy vehicle fuel cell engine, Int J Hydrogen Energy:https://doi.org/10.1016/jijhydene.2019.10.134.
16. Bao C, Ouyang M, Yi B. Modeling and optimization of the air system in polymer exchange membrane fuel cell systems. J Power Sources 2006;156(2):232e43. https://doi.org/10.1016/j.jpowsour.2005.06.008.
17. Gelfi S, Stefanopoulou AG, Pukrushpan JT, Peng H. Dynamics of low-pressure and high-pressure fuel cell air supply systems. In: Proceedings of the 2003 American control conference, 2003, vol. 3. IEEE; 2003. p. 2049e54.
18. Tafaoli-Masoule M, Shakeri M, Esmaili Q, Bahrami A. Pem fuel cell modeling and pressure investigation. Energy Source Part A 2011;33(24):2291e302. https://doi.org/10.1080/15567030903530566.
19. Ahmadi N, Dadvand A, Rezazadeh S, Mirzaee I. Analysis of the operating pressure and gdl geometrical configuration effect on pem fuel cell performance. J Braz Soc Mech Sci Eng 2016;38(8):2311e25. https://doi.org/10.1007/s40430-016-0548-0.
20. Kim H-S, Lee D-H, Min K, Kim M. Effects of key operating parameters on the efficiency of two types of pem fuel cell systems (high-pressure and low-pressure operating) for automotive applications. J Mech Sci Technol 2005;19(4):1018e26. https://doi.org/10.1007/BF02919185.
21. Blunier B, Miraoui A. Air management in pem fuel cells: state-of-the-art and prospectives. In: 2007 International aegean conference on electrical machines and power electronics. IEEE; 2007. p. 245e54.
22. Kim DK, Min HE, Kong IM, Lee MK, Lee CH, Kim MS, Song HH. Parametric study on interaction of blower and back pressure control valve for a 80-kw class pem fuel cell vehicle. Int J Hydrogen Energy 2016;41(39):17595e615. https://doi.org/10.1016/j.ijhydene.2016.07.218.
23. Hoeflinger J, Hofmann P., Air mass flow and pressure optimisation of a PEM fuel cell range extender system, Int J Hydrogen Energy, https://doi.org/10.1016/j.ijhydene.2020.07.176
24. Yan Q., Toghiani H., Causey H., Steady state and dynamic performance of proton exchange membrane fuel cells (PEMFCs) under various operating conditions and load changes, Journal of Power Sources 161 (2006) 492–502
25. Schroter J., et al., Influence of pressure losses on compressor performance in a ressurized fuel cell air supply system for airplane applications, International journal of hydrogen energy, 2021.
26. Hu D., et al., Optimization of speed response of super-high-speed electric air compressor for hydrogen fuel cell vehicle considering the transient current, International journal of hydrogen energy, 2021.
27. Lototskyy, M.V.; Tolj, I. ; Parsons, A. ;Smith, F.; Sita, C.; Linkov, V. Performance of electric forklift with low-temperature polymer exchange membrane fuel cell power module and metal hydride hydrogen storage extension tank, Journal of power sources 2016, 316, 239-250.

 doi:10.20944/preprints202311.0407.v1

28. A.A.Kulikovsky, "A physically-Based Analytical Polarization Curve of a PEM Fuel Cell", Journal of The Electrochemical Society, 161 (3) F263-F270 (2014).
29. S.Goessling, M. Klages, J. Haussmann, P. Beckhaus, M. Messerschmidt, T. Arlt, N. Kardjilov, I. Manke, J. Scholta, A. Heinzel, "Analysis of liquid water formation in polymer electrolyte membrane (PEM) fuel cell flow fields with a dry cathode supply", Journal of Power Sources 306, 658-665 (2016).
30. Radica G., Tolj I., Markota D., Lototskyy M.V., Pasupathi S., Yartys V.,Control strategy of a fuel-cell power module for electric forklift Share, Int J Hydrogen Energy, https://doi.org/10.1016/j.ijhydene.2021.01.225 (2021)